https://doi.org/10.1016/j.msea.2017.11.079

The Kinetic diagram of sigma phase and its precipitation hardening effect on 15Cr-2Ni duplex stainless steel

Jianquan Wan, Haihui Ruan*, Jianbiao Wang, Sanqiang Shi

Department of Mechanical Engineering, The Hong Kong Polytechnic University, Hung Hom, Kowloon, Hong Kong, China

Abstract

The kinetics of sigma phase precipitation at the temperature range of 750~950 °C in a rapidly solidified 15Cr-2Ni-2Al-11Mn resource-saving duplex stainless steel was investigated. After fitting the experimental results with the Avrami equation, the TTT diagram of sigma phase was established. It is found that the precipitation rate of sigma phase maximizes at about 850 °C and that the precipitation hardening effect sharply peaks at about 1.5 vol.% sigma phase content, which is obtained by aging at 850 °C for 180 minutes. With the further increase of sigma phase content from 1.5 vol.%, the strength reduces and the ductility increases again.

Keywords: Duplex stainless steel; TTT diagram; Precipitation hardening; Mechanical strength

* Corresponding author: Tel./fax: + 852 2766 6648.
E-mail address: haihui.ruan@polyu.edu.hk

1. Introduction

Duplex stainless steel (DSS) is composed of both ferrite (δ) and austenite (γ) phases, and exhibits an excellent combination of mechanical property and corrosion resistance [1, 2], which is thus increasingly used in stringent environment [3-7]. DSS can be precipitation hardened by sigma (σ) phase at the expense of plasticity and toughness [8]. Several precipitation reactions can occur during the aging temperature of 600~1000 °C, leading to the formation of intermetallic compounds such as σ, χ, $M_{23}C_6$, Cr_2N, etc. [9], among which σ phase deteriorates most on the toughness as well as the corrosion resistance. The hardness of σ phase is high to about 17 GPa at the peak load of 500 μN by using nanoindentation [10], and it is a non-magnetic intermetallic phase consisted mainly with iron and chromium. The diffusion velocity of the σ phase forming elements in δ phase is faster than that in γ phase, and the precipitation rate of the σ phase in δ phase is nearly about 100 times as that of γ phase [11]. Growing proper size and amount of σ phase through aging is mostly used to develop precipitation hardening in DSS. It relies on the temperature-dependent solid solubility to produce fine particles of intermetallic compound, which impedes the movement of dislocations or other defects in the crystal lattice. The σ phase is formed in DSS during annealing at 550-950 ºC, so the application of DSS is usually limited to temperature not exceeding 500 °C. The hardening effect of σ phase precipitate on the mechanical property of stainless steel depends on the factors such as the size, morphology, volume fraction and distribution of σ phase in the matrix [10].

The kinetics of σ phase precipitation were subjected to extensive investigations.

Kim *et al.* [12] studied the precipitation behavior of σ phase in cast DSS CD3MN and CD3MWCuN, and established the time-temperature-transformation (TTT) diagram of σ phase. The effects of plastic deformation [13-16] and alloying elements [17-20] were investigated to reveal the basic mechanism of σ phase precipitation in stainless steel. It was found that both the decreased grain size [21] and high crystallographic misorientation between the γ and δ phases [22] promote σ phase precipitation. The effect of σ phase precipitation on the mechanical performance of stainless steel were also investigated and well in progress. Some early reports showed that creep strength is reduced by the presence of σ phase [23-25], and the dendrite of σ phase leads to embrittlement of stainless steel [26]. However, recent investigations indicated that σ phase can also be beneficial for mechanical property. Plastic deformation can be used to refine the σ phase particles into stable globular morphology. The fine and homogeneous dispersion of σ phase can play a role of precipitation strengthening in DSS alloys [27, 28], and it improves the creep strength [29] and plasticity [30] of DSS alloys. Shek *et al.* [31, 32] found that the strength and ductility of 25Cr-8Ni DSS can be enhanced when the distribution and morphology of σ phase are properly controlled through appropriate heat treatment and that the hot tensile strength of aged samples is higher than those of unaged ones since the ($\sigma + \gamma_2$) structure behaves like a reinforcing phase. Pohl *et al.* [33] reported that σ phase precipitation of 1 vol.% leads to two thirds reduction of impact toughness and that the strengthening effect of σ phase peaks at about 18 vol.% without considering the variation of γ phase content.

Understanding the impact of σ phase precipitation on the mechanical performance

is crucial to the development of high performance DSS. This work establishes the TTT diagram of σ phase after the non-equilibrium kinetics diagram of γ phase was established in previous work [34], and then the quantitative relation between σ phase and the mechanical property of DSS is sought.

2. Experimental

The raw materials were melted in an electric arc furnace and then fast solidified into a copper mould at room temperature, which resulted in about 70% δ phase in the as-cast alloy. The specific chemical composition of the casting alloy was obtained through spectroscopic analysis and shown in Table 1. Cold-rolled (70% thickness reduction) samples were then annealed at 750~ 950 ºC for different time followed by water quenching, respectively. The centre region of the DSS samples was examined in order to avoid any surface effect. Samples were electrolytically etched in 15 wt.% KOH solution, which makes the γ bright, δ gray and σ reddish brown under an optical microscope. The optical images from ten randomly selected areas of the etched surface were taken using a 500x objective lens in order to analyze the volume fraction of σ phase using the metallography image analysis software. Selected sample was subjected to investigation using transmission electron microscope (TEM, JEOL 2000FX working at 200 kV) to identify σ phase. The sample was thinned into 30 μm by sand paper, punched into wafers of 3 mm diameter and ion milled to get the TEM foils. For tensile test, all samples were wire-cut into dog-bone shape with the gauge dimension of 5×30×1 mm, to which a 25-mm extensometer can be attached for an accurate measurement of the elongation. The fracture surface of samples after tensile

test were observed using a Jeol 6490 scanning electron microscope (SEM).

Corrosion behavior of the aged DSS samples was investigated based on potentiodynamic polarization curves. Polarization test was conducted using potentiodynamic polarization electrochemical methods and evaluated in the solution of 3.5 wt.% NaCl at 25 °C. The experiments were carried out in a 200 ml conventional three-electrode cell comprising the sample as the working electrode, a Pt foil as the auxiliary electrode and a saturated calomel electrode as the reference one. Prior to testing, samples were mechanically polished from 240 to 1200 grit abrasive paper, washed with distilled water, degreased with acetone and dried in air. The interface between sample and resin was coated with a polyacrylate quick-setting resin to avoid the possibility of crevice corrosion during measurement. Polarization test of each sample was performed at least three times using a Potentiostat/Galvanostat (EG&G Princeton Applied Research, Model 273A).

3. Results

3.1 The microstructure of σ phase

Fig. 1(a) (c) (d) show the DSS samples aging at 750 ºC for 360 min and 900 ºC for 45min and 90 min followed by water quenching, respectively. The matrix of samples shows an obvious duplex structure of δ and γ phase, and σ phase was found in γ phase. No σ phase was found in the sample aging at 950 ºC. Fig. 1(b) shows the SEM image of the DSS sample aging at 750 ºC for 1050 min followed by water quenching and the chemical composition of σ, δ and γ phases obtained using the energy dispersive X-ray

spectroscopy (EDS) is listed in Table 2. It is noted that the chemical composition of σ phase is more close to that of γ phase than that of δ phase. The size of σ phase increases with aging time and temperature. The morphology of σ phase changes with aging temperature. At 750 °C, a coral-like structure of σ phase forms, while that of 900 °C is bulk-like σ phase. At 750 °C, the high local supersaturation of parent solid solutions provides a high thermodynamic driving force for σ phase precipitation, leading to a high rate of nucleation; however, the low diffusion rate hinders the growth of σ phase precipitates. While for 900 °C, the size of σ phase is big and the linking between single σ crystals is marginal, due to the low nucleation formation force but a high diffusion rate [33]. The volume fraction of σ phase precipitated in DSS sample as a function of aging time is shown in the dot symbol of Fig. 2. The volume fraction of σ phase increases with aging time, and reaches a steady value after a sufficiently long aging time. From 750 to 850 °C, the maximum volume fraction of σ phase shows an increase from 9.5% to 11.5%, but at 900 °C the maximum volume fraction was approximately 10.5%.

3.2 The precipitation kinetics of σ phase in DSS

The Johnson–Mehl–Avrami (JMA) relationship is one of the most commonly used theories to describe the kinetics of σ phase precipitation in many systems involving nucleation and growth, and it is shown as follows:

$$f = \phi / \phi^e = 1 - \exp(-kt^n)$$

Where f is the transformed ratio, ϕ^e is the volume fraction of σ phase at the equilibrium state, ϕ is the volume fraction of σ phase at time t, k and n are fitting parameters. The magnitudes of fitting parameters k, n, ϕ^e are listed in Table 3. It is noted that n ≈ 2.5 is consistent with the kinetics of σ phase precipitation in [12], which indicates that σ phase precipitation is diffusion controlled. Fig. 2 shows the aging experimental data and fitting curves of the temperature-time dependent variation of σ phase content, which exhibits the non-equilibrium kinetic and the equilibrium state of the σ phase precipitation in DSS samples. For short time aging, the volume fraction of σ phase is so small that σ phase can not be distinguished from the optical or SEM image, so TEM test was used to validate the fitting line on short time aging. For DSS sample aged at 750 ºC for 90 min, the predicted volume fraction of σ phase is about 0.1 %, and a σ phase grain with a size approximately 200 nm was found as shown in Fig. 3. The Avrami equations were then used to establish TTT diagrams of volume fraction of σ phase and transformed ratio f of σ phase for f = 1%, 50% and 99% as shown in Fig. 4. Usually, the time needed for f = 1% is defined as the breeding time, while f = 99% as completed. It is learned that the breeding time is the largest at 750 ºC, which is consistent with the understanding that the nucleation rate is larger at the lower temperature. It can be seen that the nose of the TTT curves is located at 850 ºC, which indicates that DSS samples have the fastest precipitation rate of σ phase at 850 ºC. For the DSS in this work, the content of γ phase increased with aging temperature in 750~900 ºC since the as-cast DSS samples were fast-solidified and cold-rolled with 70% plastic deformation [34]. This is distinct from

the conventional notion that γ phase content decreases with heat treatment temperature. In addition, it is observed that σ phase mainly precipitates in γ phase. Therefore, the effect of γ phase content could be nontrivial. High aging temperature in 750~900 ºC increases the content of γ phase, and it facilitates the formation of σ phase. On the other hand, high aging temperature reduces the potential number of nucleation sites due to the increased grain size of primary phase, which in turn reduces the tendency of σ phase formation. The competition of these two effects could lead to the nose in the TTT diagram of σ phase as shown in Fig. 4(a).

3.3 Precipitation hardening effect of σ phase on the mechanical property of DSS

Tensile test was conducted on the DSS samples aging at 850 ºC for different time to investigate the effect of σ phase precipitation on the mechanical performance. Fig. 5 shows the tensile curves of DSS samples aging at 850 ºC for 105, 140, 160, 180,195, 210, 235 min, respectively, and the variation on the ultimate tensile strength (UTS) and elongation of DSS samples were shown in Fig.6. It shows that DSS sample aging for 105 min exhibits normal mechanical performance with UTS about 555 MPa and elongation 28% in 15Cr-2Ni series DSS. With the aging time increases, the UTS increases while elongation decreases. The UTS reaches a peak of about 920 MPa meanwhile with the worst elongation no more than 5% for sample aging 180 min. Aging longer than 180 min, the UTS decreases while elongation increases with aging time. The volume fraction of γ phase increases with the aging time, and reaches a steady value of about 50% at 180 min and will not change with longer aging time as investigated in [34]. In the range of aging time 105, 140, 160 and 180 min, the UTS

should decrease while elongation increase due to the increase of ductile γ phase in DSS samples. Meanwhile, the σ phase content increase from 0.44% to 0.84%, 1.13% and 1.46% according to aging experiment result, and it exhibits increasing hardening effect far exceeding the softening effect of γ phase. Therefore, the UTS of DSS samples increases with aging time before 180 min. In the range of aging time 180, 195, 210 and 235 min, the volume fraction of γ phase in DSS samples is nearly the same, but the grain size of δ and γ phases increases with aging time. So the UTS of DSS samples should decrease while elongation increases. The σ phase content of DSS samples aging for 180, 195, 210 and 235 min is 1.46%, 1.74%, 2.03% and 2.57%, respectively, and it exhibits much smaller impact on the mechanical performance of DSS than that of primary phase grain size. Therefore, the UTS of DSS samples decreases with aging time after 180 min.

It is noted that the peak hardening effect occurs at 1.46 vol.% σ phase content at 850 ºC. This is notably different from the experiment result of DSS alloy with high Cr content investigated by Pohl *et al.* [33], in which the peak hardening occurs at 18 vol.% σ phase. The reinforcing phase is solely σ phase instead of the (σ + γ_2) structure, which provides strong hardening effect on the mechanical performance of DSS in this work.

3.4 The effect of Mo on the kinetics of σ phase precipitation

The effect of Mo on the precipitation behavior of σ phase was examined in this work by adding 0.5 wt.% and 1 wt.% Mo. In this section, the Mo-free and the two additional DSS samples were referred as Mo-0, Mo-0.5 and Mo-1, respectively. The

aging data were fitted using the JMA equation, and the magnitudes of fitting parameters k, n, ϕ^e are listed in Table 4. Fig. 7 shows the experimental results and fitting curves of Mo-0, Mo-0.5 and Mo-1 on the time-dependent variation of σ phase content at 850 ºC. It was found that both the precipitation rate and the equilibrium content of σ phase increase with the addition of Mo.

Fig. 8 shows the metallographs of Mo-0, Mo-0.5, Mo-1 DSS samples aged at 850 ºC for 780 min. It is noted that the size and amount of σ phase increases with Mo content. For Mo-0.5 and Mo-1, most of σ phase was formed in δ phase, and it is in sharp contrast to the case of Mo-0 of which σ phase was formed in γ phase. It is consistent with conventional notion that Mo not only stabilizes δ phase but also promotes the σ phase formation in δ phase. It should be stressed that the addition of Mo could change the precipitation mechanism and brings about completely different hardening effect. In the case Mo-0, σ phase precipitates in the ductile γ phase, leading to the strong hardening effect as shown in Fig. 5. However, if it precipitates in the δ phase due to the addition of Mo, the hardening effect could be much smaller, as reported in [33, 35].

4. Discussion

4.1 The mechanism of σ phase precipitation on strengthening DSS

Intuitively, the σ phase precipitation prevents the dislocation movement, therefore increases the strength of DSS. However, the UTS of DSS shows an increase-decrease variation when the aging time increases, as shown in Fig. 6. With the aging time

longer than 180 min, the formation rate of σ phase decreases as shown in the fitting curve of Fig.2, but the grain size of σ phase increases. The coarsened σ phase precipitation does not inhibit sufficiently to the mobile dislocations, leading to the decreased UTS of DSS sample aged for 195 min and longer. This is the over aging mechanism [36] which is common in metal alloys though there is also some abnormal cases [10]. The effect of aging can be attributed to the change on the morphology of σ phase. The UTS increases with linking of σ phase particles, and decreases with more bulk σ phase particles [33]. With the increase of aging time in 105~180 min, the fine σ phase particles aggregate to form a net-like structure, leading to an apparent strengthening effect. However, the pinned high-density dislocations result in cracks and reducing ductility. Cracks are able to run through σ phase network over long distance. Even little deformation of the DSS sample can cause transcrystalline fracture of σ phase network due to the topologically close-packed (TCP) structure of σ phase, and finely structured σ phase particles are formed [33, 37]. Therefore, at the critical content of σ phase with the maximum hardening effect, small deformation of DSS sample can cause the fracture on the matrix of DSS sample. While for long time aging, the more bulk-like σ phase is associated with the larger δ and γ grains. The bulky and hard σ phase causes the deflection of cracks, which can even make the surrounding brittle δ phase failure in a more ductile mode [33]. Above analysis was confirmed by the typical morphology on the fracture surface of DSS samples aged at 850 ºC for 105, 180 and 235 min after tensile test at room temperature as shown in Fig. 9. The morphology of samples aged for 105 min and 235 min show most ductile fracture

feature, composed of fine and big ductile dimples which contributed to the ductility. However, sample aged for 180 min shows most brittle fracture feature, and σ phase precipitation was identified at the fracture surface with the chemical composition listed in Table 5. Apparently, σ phase plays the role of crack source and leads to the brittleness of the sample aged for 180 min.

4.2 The effect of σ phase precipitation on the corrosion resistance of DSS

The hardening effect of σ phase is associated with the degradation of corrosion resistance of DSS, which needs attention. These DSS samples, which were used in pitting corrosion test, were aged at 850 ºC for 30, 90, 180 and 320 min respectively, followed by water quenching. Fig. 10(a) shows the representative polarization curves of DSS samples in 3.5 wt.% NaCl aqueous solution at 25 °C. The pitting potential values are exhibited in Fig. 10(b), and it is reduced with the increase of σ phase content. It is consistent with other reports [38, 39]. Therefore, for gaining higher mechanical strength of DSS, the corrosion resistance is compromised. It is proper for some low corrosive applications. It is known that corrosion pits provide initiation sites for fatigue cracks and stress corrosion cracks [40]. But a proper amount of σ phase was reported to improve the corrosive wear behavior of stainless steels in sulphuric acid [41].

5. Conclusion

The kinetics of σ phase precipitation and its hardening effect on the mechanical property of DSS alloy were investigated and the main findings are as follows:

1. Upon aging at 750~900 ºC, the σ phase precipitates in the DSS, and the grain size of σ phase increases with aging time and temperature. The maximum volume fraction of σ phase is obtained at 850 ºC.

2. TTT diagram of σ phase precipitation is established. The nose of the TTT curves is located at 850 ºC, which indicates that the DSS sample has the fastest precipitation rate of σ phase at 850 ºC.

3. For 850 ºC aging, the hardening effect of σ phase on the strength of DSS samples increases with the volume fraction of σ phase and reaches a peak when σ phase is approximately 1.5 vol.%. Larger than it, the hardening effect is decreased due to the over aging mechanism of σ phase.

4. Mo increases the formation rate and the mass amount of σ phase, and it favors the σ phase precipitation in δ phase.

5. The corrosion resistance of DSS is reduced with the increased σ phase content, and it is compromised for gaining higher mechanical strength by precipitation hardening.

Acknowledgement

This work was supported by the Early Career Scheme (ECS) of the Hong Kong Research Grants Council (Grant No. 25200515, Account No. F-PP27). We are grateful for the support.

Reference

[1] I.N. Bastos, S.S.M. Tavares, F. Dalard, R.P. Nogueira, Effect of microstructure on corrosion behavior of superduplex stainless steel at critical environment conditions, Scripta Materialia 57(10) (2007) 913-916.

[2] T.H. Chen, K.L. Weng, J.R. Yang, The effect of high-temperature exposure on the microstructural stability and toughness property in a 2205 duplex stainless steel, Materials Science and Engineering: A 338(1–2) (2002) 259-270.

[3] H. Farnoush, A. Momeni, K. Dehghani, J.A. Mohandesi, H. Keshmiri, Hot deformation characteristics of 2205 duplex stainless steel based on the behavior of constituent phases, Materials & Design 31(1) (2010) 220-226.

[4] S. Fréchard, F. Martin, C. Clément, J. Cousty, AFM and EBSD combined studies of plastic deformation in a duplex stainless steel, Materials Science and Engineering: A 418(1–2) (2006) 312-319.

[5] J.-O. Nilsson, Super duplex stainless steels, Materials science and technology 8(8) (1992) 685-700.

[6] P. Sathiya, S. Aravindan, R. Soundararajan, A. Noorul Haq, Effect of shielding gases on mechanical and metallurgical properties of duplex stainless-steel welds, Journal of Materials Science 44(1) (2009) 114-121.

[7] J. Charles, Duplex stainless steels, a review after DSS'07 in Grado, Revue de Metallurgie 105(3) (2008) 155-171.

[8] J. Lee, I. Kim, A. Kimura, Application of small punch test to evaluate sigma-phase embrittlement of pressure vessel cladding material, Journal of nuclear science and technology 40(9) (2003) 664-671.

[9] C.-S. Huang, C.-C. Shih, Effects of nitrogen and high temperature aging on σ phase precipitation of duplex stainless steel, Materials Science and Engineering: A 402(1) (2005) 66-75.

[10] Y. Wang, J. Han, B. Yang, X. Wang, Strengthening of σ phase in a Fe20Cr9Ni cast austenite stainless steel, Materials Characterization 84 (2013) 120-125.

[11] E. Baerlecken, H. Fabritius, Umwandlungskinetik der Sigmaphase in einer Eisen‐Chrom‐Legierung mit 48% Cr, steel research international 26(11) (1955) 679-686.

[12] Y.-J. Kim, L.S. Chumbley, B. Gleeson, Determination of isothermal transformation diagrams for sigma-phase formation in cast duplex stainless steels CD3MN and CD3MWCuN, Metallurgical and Materials Transactions A 35(11) (2004) 3377-3386.

[13] P. Duhaj, J. Ivan, E. Makovicky, Sigma-Phase Precipitation in Austenitic Steels, J Iron Steel Inst 206(12) (1968) 1245-1251.

[14] C. Huang, H. Chen, A discussion on stainless steels welding (II), Welding and Cutting 8 (1998) 48-54.

[15] S. Zormalia, T. Koutsoukis, E. Papadopoulou, P. Kokkonidis, G. Fourlaris, Effect of ageing in cold rolled superaustenitic stainless steels, EMC 2008 14th European Microscopy Congress 1–5 September 2008, Aachen, Germany, Springer, 2008, pp. 451-452.

[16] C.-C. Hsieh, D.-Y. Lin, W. Wu, Precipitation behavior of σ phase in 19Cr–9Ni–2Mn and 18Cr–0.75 Si stainless steels hot-rolled at 800° C with various reduction ratios, Materials Science and Engineering: A 467(1) (2007) 181-189.

[17] Y. Maehara, Y. Ohmori, J. Murayama, N. Fujino, T. Kunitake, Effects of alloying elements on σ phase precipitation in δ–γ duplex phase stainless steels, Metal Science 17(11) (1983) 541-548.

[18] J. Charles, Super duplex stainless steels: structure and properties, Proc. Conf. Duplex Stainless

Steels' 91, 1991, pp. 3-48.
[19] K. Shinohara, T. Seo, K. Kumada, Recrystallization and sigma phase formation as concurrent and interacting phenomena in 25% Cr-20% Ni steel, Transactions of the Japan Institute of Metals 20(12) (1979) 713-723.
[20] D.M.E. Villanueva, F.C.P. Junior, R.L. Plaut, A.F. Padilha, Comparative study on sigma phase precipitation of three types of stainless steels: austenitic, superferritic and duplex, Materials Science and Technology 22(9) (2006) 1098-1104.
[21] K. Shobu, Computer Coupling of Phase Diagrams and Thermochemistry, (2008).
[22] Y.S. Sato, H. Kokawa, Preferential precipitation site of sigma phase in duplex stainless steel weld metal, Scripta Materialia 40(6) (1999) 659-663.
[23] G.J. Guarnieri, J. Miller, F.J. Vawter, The Effect of Sigma Phase on the Short-Time High Temperature Properties of 25 Chromium-20 Nickel Stainless Steel, Trans. ASM 42 (1950) 981.
[24] J. Lai, A. Wickens, Effect of intergranular particle size and spacing on creep ductility of type 316 stainless steel, Scripta Metallurgica 13(12) (1979) 1197-1198.
[25] C. McMahon, On the mechanisms of creep damage in type 316 stainless steel, Scripta Metallurgica 19(6) (1985) 733-737.
[26] T. Gill, M. Vijayalakshmi, J. Gnanamoorthy, K. Padmanabhan, Transformation of Delta-Ferrite During the Postweld Heat Treatment of Type 316 L Stainless Steel Weld Metal, Weld. J. 65(5) (1986) 122.
[27] C. Shek, K. Wong, J. Lai, Review of temperature indicators and the use of duplex stainless steels for life assessment, Materials Science and Engineering: R: Reports 19(5-6) (1997) 153-200.
[28] J. Lai, K. Wong, D. Li, Effect of solution treatment on the transformation behaviour of cold-rolled duplex stainless steels, Materials Science and Engineering: A 203(1-2) (1995) 356-364.
[29] D. Li, Y. Gao, J. Tan, F. Wang, J. Zhang, Effect of σ-Phase on the creep properties of Cr25Ni20 stainless steel, Scripta metallurgica 23(8) (1989) 1319-1321.
[30] Y.S. Han, S.H. Hong, The effects of thermo-mechanical treatments on superplasticity of Fe-24Cr-7Ni-3Mo-0.14 N duplex stainless steel, Scripta materialia 36(5) (1997) 557-563.
[31] C. Shek, D. Li, K. Wong, J. Lai, Creep properties of aged duplex stainless steels containing σ phase, Materials Science and Engineering: A 266(1) (1999) 30-36.
[32] C. Shek, K. Wong, J. Lai, D. Li, Hot tensile properties of 25Cr-8Ni duplex stainless steel containing cellular (σ+ γ 2) structure after various thermal treatments, Materials Science and Engineering: A 231(1) (1997) 42-47.
[33] M. Pohl, O. Storz, T. Glogowski, Effect of intermetallic precipitations on the properties of duplex stainless steel, Materials characterization 58(1) (2007) 65-71.
[34] J. Wan, H. Ruan, S. Shi, Excellent combination of strength and ductility in 15Cr-2Ni duplex stainless steel based on ultrafine-grained austenite phase, Materials Science and Engineering: A 690(Supplement C) (2017) 96-103.
[35] C.H. Shek, K.W. Wong, J.K.L. Lai, D.J. Li, Hot tensile properties of 25Cr-8Ni duplex stainless steel containing cellular (σ+γ2) structure after various thermal treatments, Materials Science and Engineering: A 231(1) (1997) 42-47.
[36] T. Karahan, H.E. Emre, M. Tümer, R. Kaçar, Strengthening of AISI 2205 duplex stainless steel by strain ageing, Materials & Design 55 (2014) 250-256.
[37] R.A. Donald, P.P. Pradeep, D.K. Bhattacharya, Essentials of Materials Science and Engineering[M] (2004).

[38] K. Ravindranath, S.N. Malhotra, Influence of Aging on Intergranular Corrosion of a 25% Chromium-5% Nickel Duplex Stainless Steel, CORROSION 50(4) (1994) 318-328.
[39] V. Moura, L. Lima, J. Pardal, A. Kina, R. Corte, S. Tavares, Influence of microstructure on the corrosion resistance of the duplex stainless steel UNS S31803, Materials Characterization 59(8) (2008) 1127-1132.
[40] J.O. Nilsson, Super duplex stainless steels, Materials Science and Technology 8(8) (1992) 685-700.
[41] X.-C. Lu, S. Li, X. Jiang, Effects of σ phase in stainless steels on corrosive wear behavior in sulfuric acid, Wear 251(1) (2001) 1234-1238.

List of Captions

Table 1 The specific chemical compositions of 15Cr-2Ni DSS (wt.%).

Table 2 The chemical composition of σ, δ and γ of DSS sample aging at 750 ºC for 1050 min (wt.%).

Table 3 Fitting parameters of Avrami equation for DSS sample aging at 750, 850 and 900 ºC.

Table 4 Fitting parameters of Avrami equation for Mo-0, Mo-0.5, Mo-1 aging at 850 ºC.

Table 5 The chemical composition of σ phase on the fracture surface of DSS sample aging at 850 ºC for 180 min (wt.%).

Fig.1 DSS samples aging at 750 ºC for (a) 360 min and 900 ºC for (c) 45 min (d) 90 min followed by water quenching, respectively. (b) Scanning electron micrograph on the DSS sample aging at 750 ºC for 1050 min followed by water quenching.

Fig. 2 Aging data and fitting curves of DSS sample on the temperature-time dependent variation of σ phase content.

Fig.3 The typical TEM images taken from δ/γ interface of DSS sample aging at 750 ºC for 90 min followed by water quenching.

Fig. 4 TTT diagram of (a) volume fraction of σ phase and (b) transformed ratio f of σ phase.

Fig. 5 Tensile curves for DSS samples aging at 850 ºC for 105, 140, 160, 180, 195, 210, 235 min followed by water quenching, respectively.

Fig. 6 Variation on the ultimate tensile strength and elongation of DSS samples aging at 850 ºC for 105, 140, 160, 180, 195, 210, 235 min followed by water quenching, respectively.

Fig. 7 Aging data and fitting curves of Mo-0, Mo-0.5 and Mo-1 on the time dependent variation of σ phase content at 850 ºC.

Fig. 8 Metallographs of DSS samples aging at 850 ºC for 780 min followed by water quenching (a) Mo-0, (b) Mo-0.5 and (c) Mo-1

Fig. 9 The typical morphology on the fracture surface of DSS samples aging at 850 ºC for (a) 105, (b)180 and (c) 235 min followed by water quenching, respectively.

Fig. 10 Pitting corrosion resistance of DSS samples in 3.5 wt.% NaCl aqueous solution at 25 ºC (a) Polarization curves (b) Pitting potential values. These DSS samples were aged at 850 ºC for 30, 90, 180 and 320 min respectively, followed by water quenching.

Figure(s)

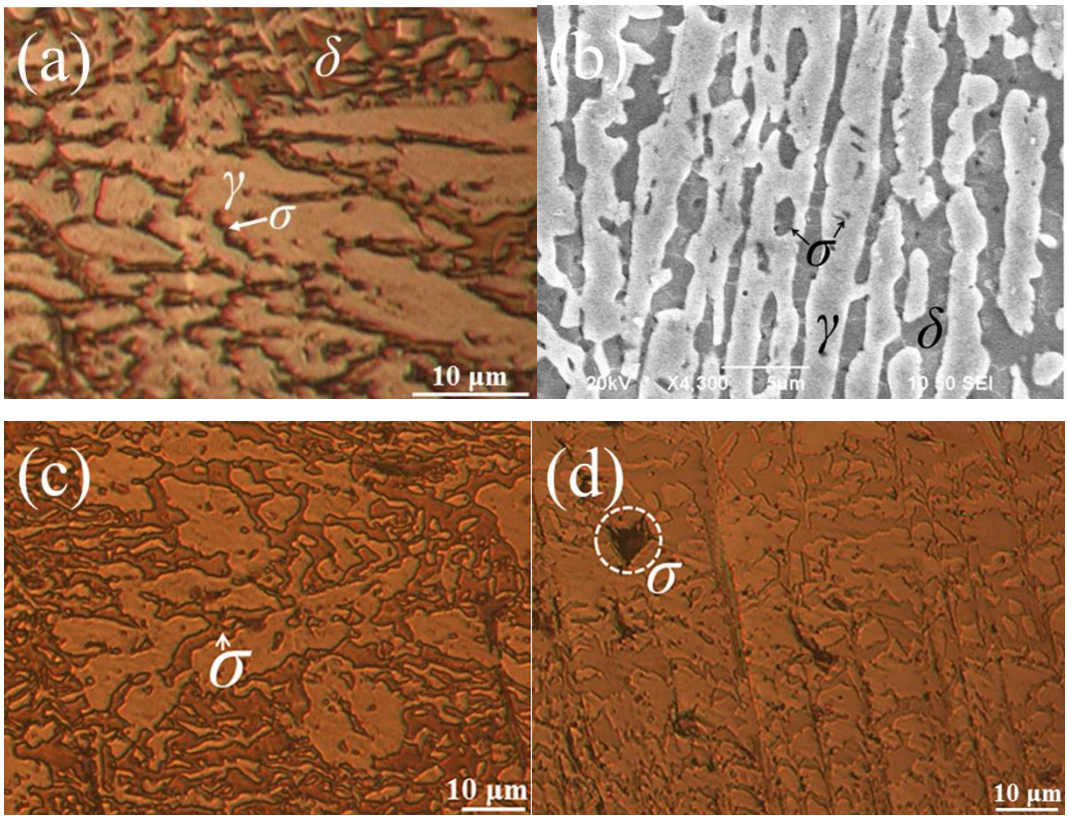

Fig.1 DSS samples aging at 750 ºC for (a) 360 min and 900 ºC for (c) 45 min (d) 90 min followed by water quenching, respectively. (b) Scanning electron micrograph on the DSS sample aging at 750 ºC for 1050 min followed by water quenching.

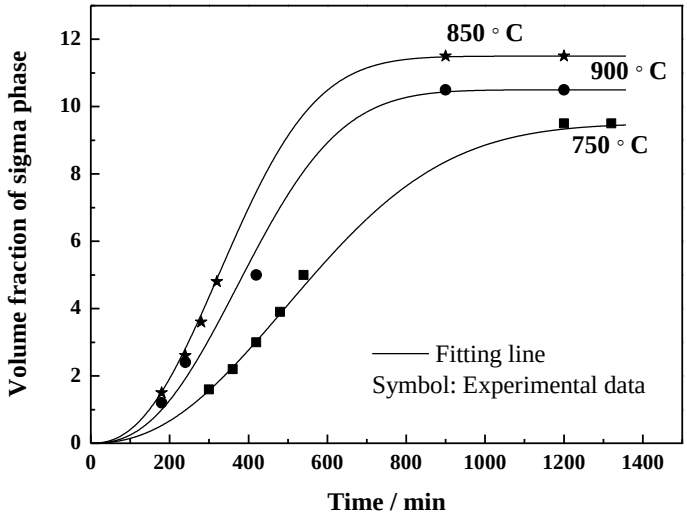

Fig. 2 Aging data and fitting curves of DSS sample on the temperature-time dependent variation of σ phase content.

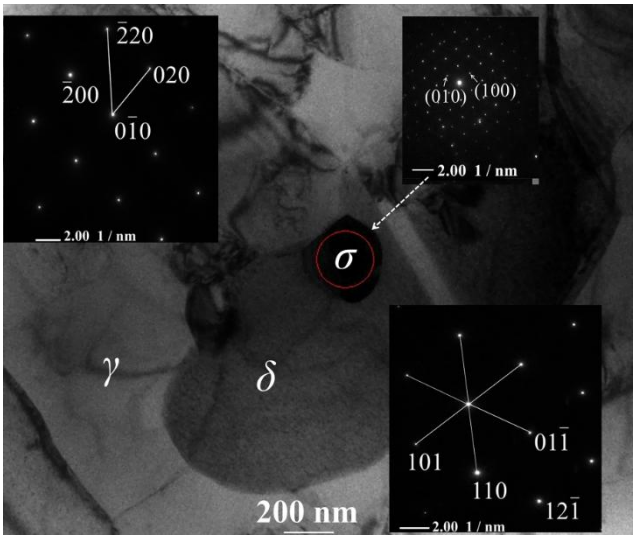

Fig.3 The typical TEM images taken from δ/γ interface of DSS sample aging at 750 ºC for 90 min followed by water quenching.

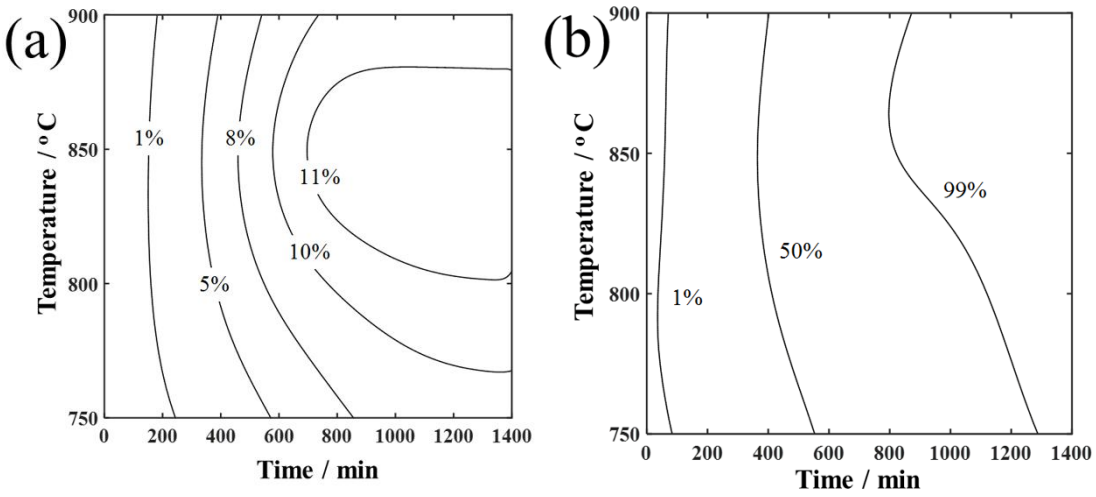

Fig. 4 TTT diagram of (a) volume fraction of σ phase and (b) transformed ratio f of σ phase.

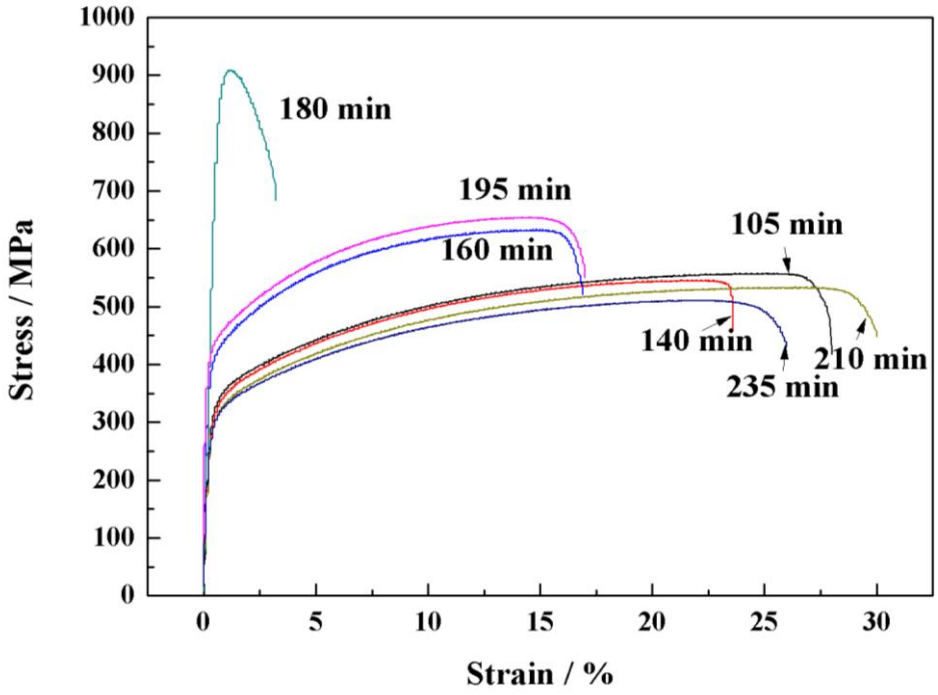

Fig. 5 Tensile curves for DSS samples aging at 850 ºC for 105, 140, 160, 180, 195, 210, 235 min followed by water quenching, respectively.

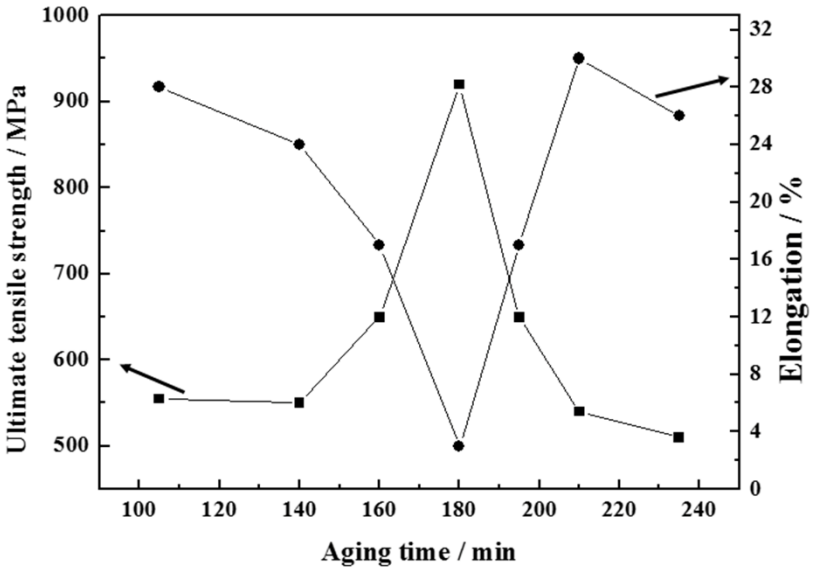

Fig. 6 Variation on the ultimate tensile strength and elongation of DSS samples aging at 850 ºC for 105, 140, 160, 180, 195, 210, 235 min followed by water quenching, respectively.

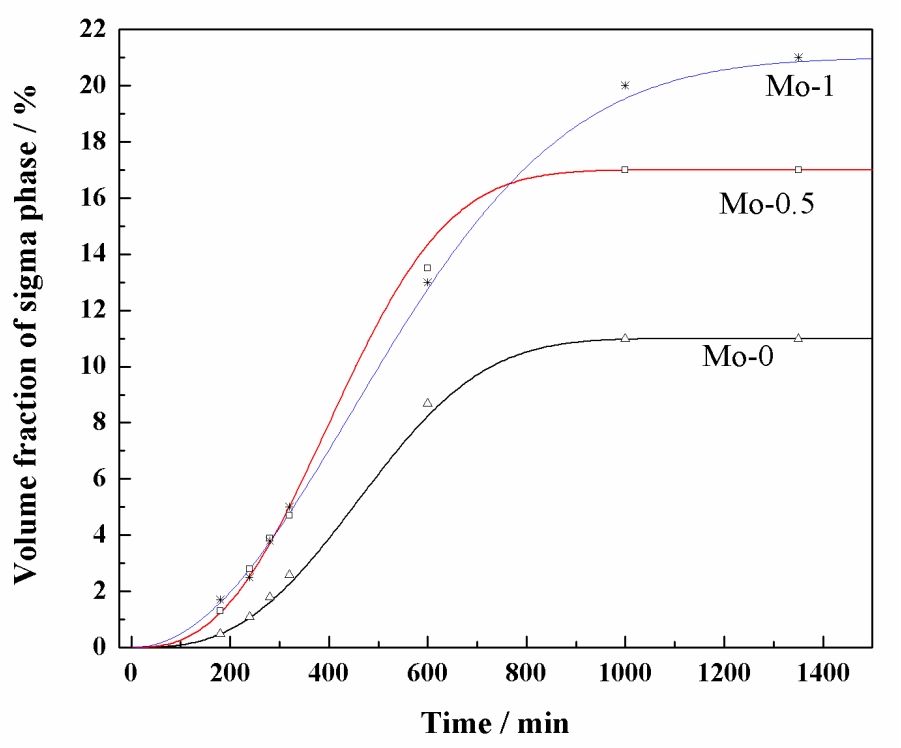

Fig. 7 Aging data and fitting curves of Mo-0, Mo-0.5 and Mo-1 on the time dependent variation of σ phase content at 850 ºC.

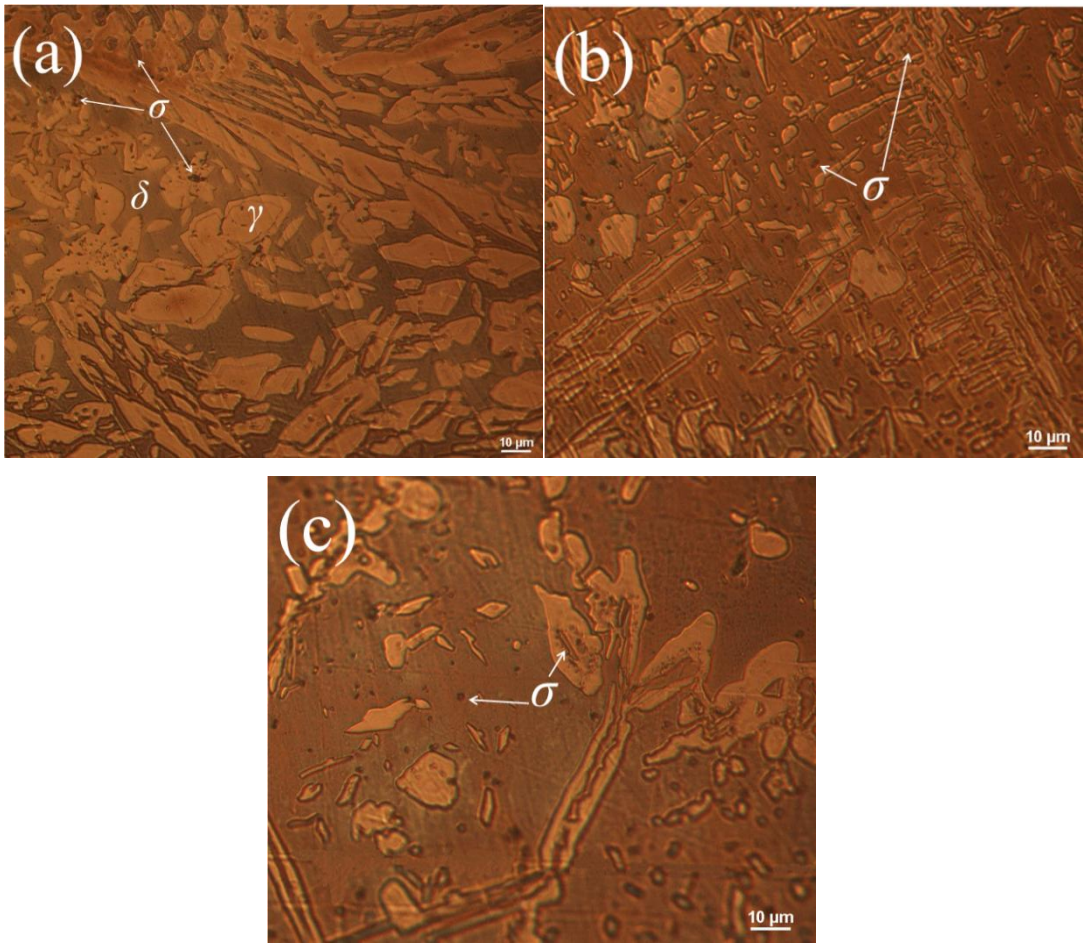

Fig. 8 Metallographs of DSS samples aging at 850 ºC for 780 min followed by water quenching (a) Mo-0, (b) Mo-0.5 and (c) Mo-1

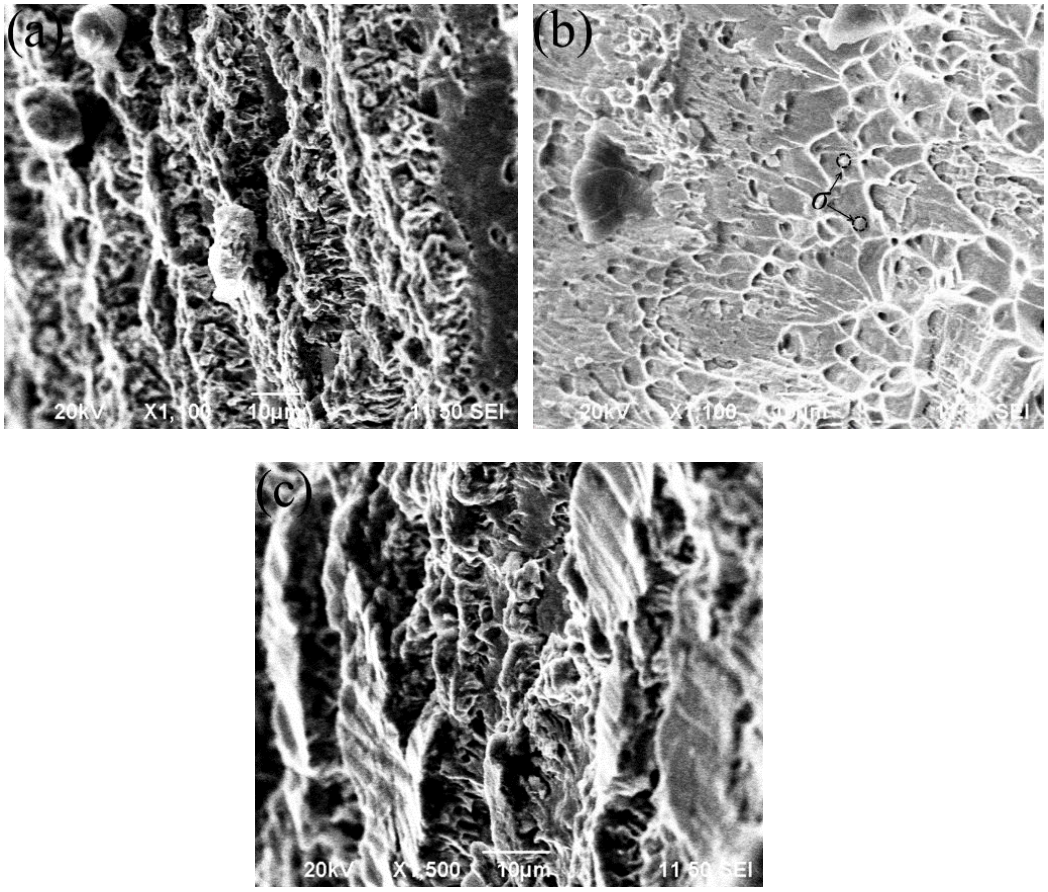

Fig. 9 The typical morphology on the fracture surface of DSS samples aging at 850 ºC for (a) 105, (b)180 and (c) 235 min followed by water quenching, respectively.

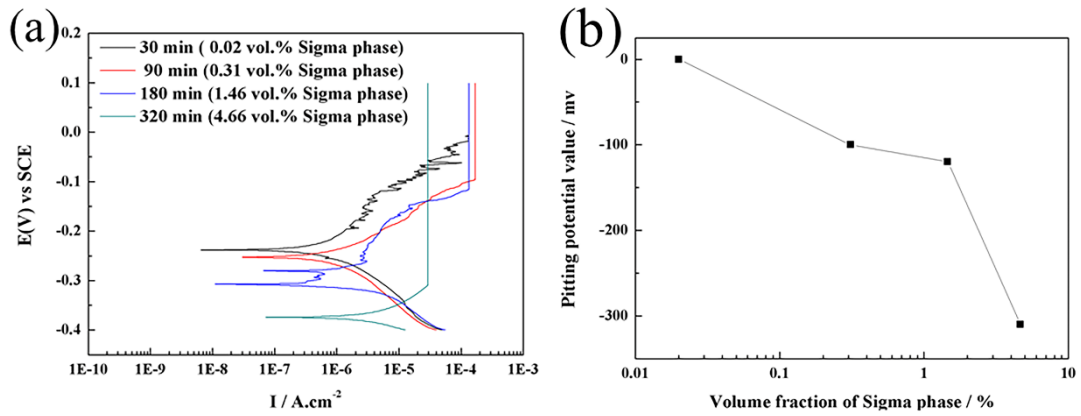

Fig. 10 Pitting corrosion resistance of DSS samples in 3.5 wt.% NaCl aqueous solution at 25 ºC (a) Polarization curves (b) Pitting potential values. These DSS samples were aged at 850 ºC for 30, 90, 180 and 320 min respectively, followed by water quenching.

Table(s)

Table 1 The specific chemical compositions of 15Cr-2Ni DSS (wt.%).

Element	Fe	Cr	Al	Ni	Mn	C
wt.%	Balance	15.27	1.96	2.04	11.05	0.02

Table 2 The chemical composition of σ, δ and γ phases of DSS sample aging at 750 ℃ for 1050 min (wt.%)

	Cr	Al	Mn	Ni	Fe
δ	17.4	1	12.24	1.78	Bal.
γ	14.03	1.87	13.28	2.18	Bal.
σ	14.07	1.20	14.11	0	Bal.

Table 3 Fitting parameters of Avrami equation for DSS sample aging at 750, 850 and 900 ºC

DSS	k	n	ϕ^e (%)
750 ºC	4.98E-7	2.24	9.5
850 ºC	7.46E-7	2.33	11.5
900 ºC	3.08E-7	2.44	10.5

Table 4 Fitting parameters of Avrami equation for Mo-0, Mo-0.5, Mo-1 aging at 850 ºC

DSS	k	n	ϕ^e (%)
Mo-0	7.46E-7	2.33	11.5
Mo-0.5	7.82E-8	2.65	17.0
Mo-1	1.93E-6	2.05	21.0

Table 5 The chemical composition of σ phase on the fracture surface of DSS sample aging at 850 ºC for 180 min (wt.%)

Cr	Al	Mn	Ni	Fe
14.11	7.37	9.12	0	Bal.